Electronic Supplementary Material (ESI) for Journal of Materials Chemistry A.


*Supplementary information for*

# From rational design of a new bimetallic MOF family with tunable linkers to OER catalysts

Xuan Zhang,[a] Jiangshui Luo,*[a,h,i] Kai Wan,[a] Dieter Plessers,[b] Bert Sels,[b] Jianxun Song,[c] Liugang Chen,[a,d] Ting Zhang,[e] Pengyi Tang,[e,f] Joan Ramon Morante,[f] Jordi Arbiol*[e,g] and Jan Fransaer*[a]

[a]*Department of Materials Engineering, KU Leuven, Leuven 3001, Belgium. E-mail:* jan.fransaer@mtm.kuleuven.be; jiangshui.luo@gmail.com

[b]*Centre for Surface Chemistry and Catalysis, KU Leuven, Leuven 3001, Belgium.*

[c]*Henan Province Industrial Technology Research Institute of Resources and Materials, Zhengzhou University, 450001 Zhengzhou, China;*

[d]*Henan Key Laboratory of High Temperature Functional Ceramics, Zhengzhou University, Kexue Avenue 100, Zhengzhou, 450001, China*

[e]*Catalan Institute of Nanoscience and Nanotechnology (ICN2), CSIC and BIST, Campus UAB, Bellaterra, 08193 Barcelona, Catalonia, Spain. E-mail:* arbiol@icrea.cat

[f]*Catalonia Institute for Energy Research (IREC), Jardins de les Dones de Negre 1, Sant Adrià del Besòs, 08930 Barcelona, Catalonia, Spain*

[g]*ICREA, Pg. Lluís Companys 23, 08010 Barcelona, Catalonia, Spain*

[h]*Collaborative Innovation Center of Clean Energy, Longyan University, Longyan 364012, China*

[i]*State Key Laboratory of Physical Chemistry of Solid Surfaces, Xiamen University, Xiamen 361005, China*

***Supplementary Figures and Tables:***

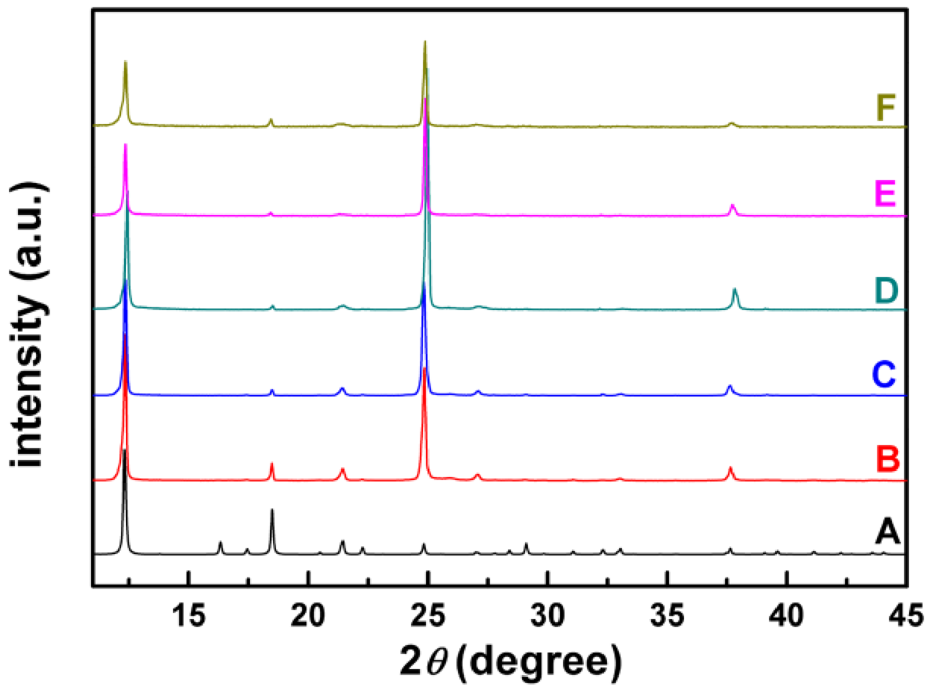


**Figure S1.** XRD patterns of simulated results for Ni-BTC-DMF (A), resultant Co-BTC-DMF (B), resultant $Co_xNi_{1-x}$-BTC-DMF-1 (C), resultant $Co_xNi_{1-x}$-BTC-DMF-2 (D), resultant $Co_xNi_{1-x}$-BTC-DMF-3 (E), and resultant Ni-BTC-DMF (F), respectively.

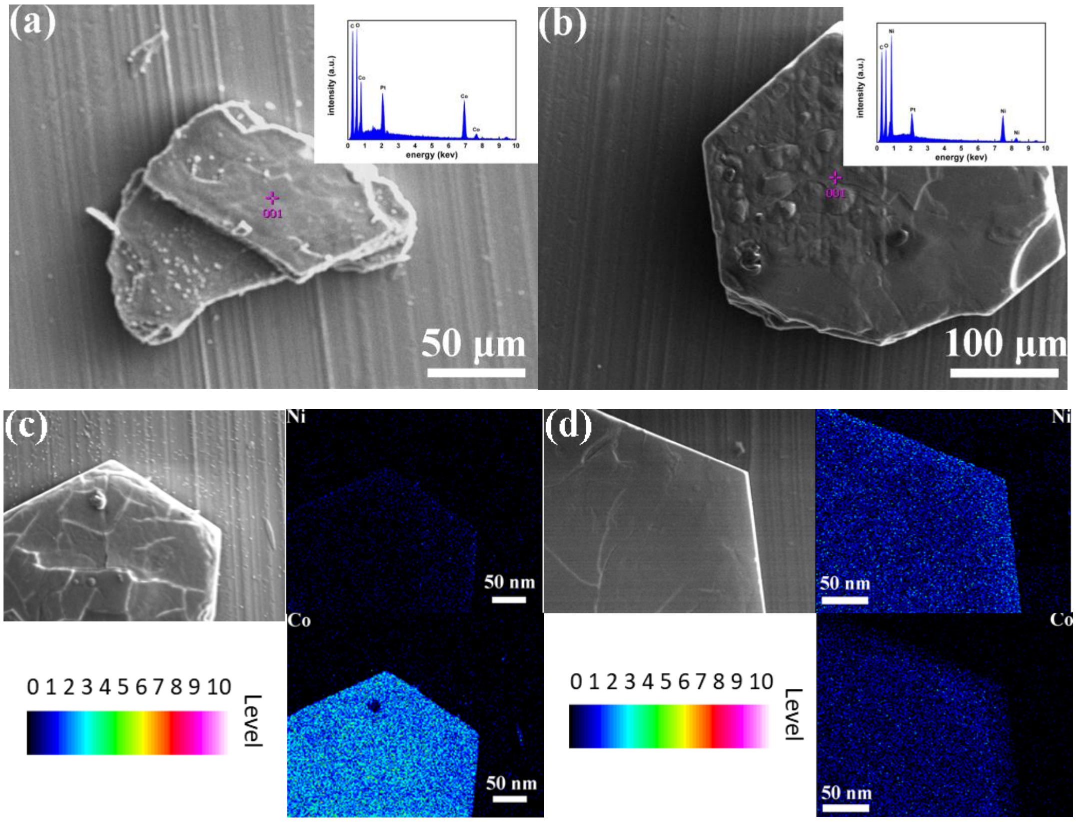


**Figure S2.** SEM images and the corresponding EMPA elemental mapping (or EDS results) for Ni-BTC-DMF (a), Co-BTC-DMF (b), $Co_xNi_{1-x}$-BTC-DMF-1 (c), and $Co_xNi_{1-x}$-BTC-DMF-3 (d), respectively.

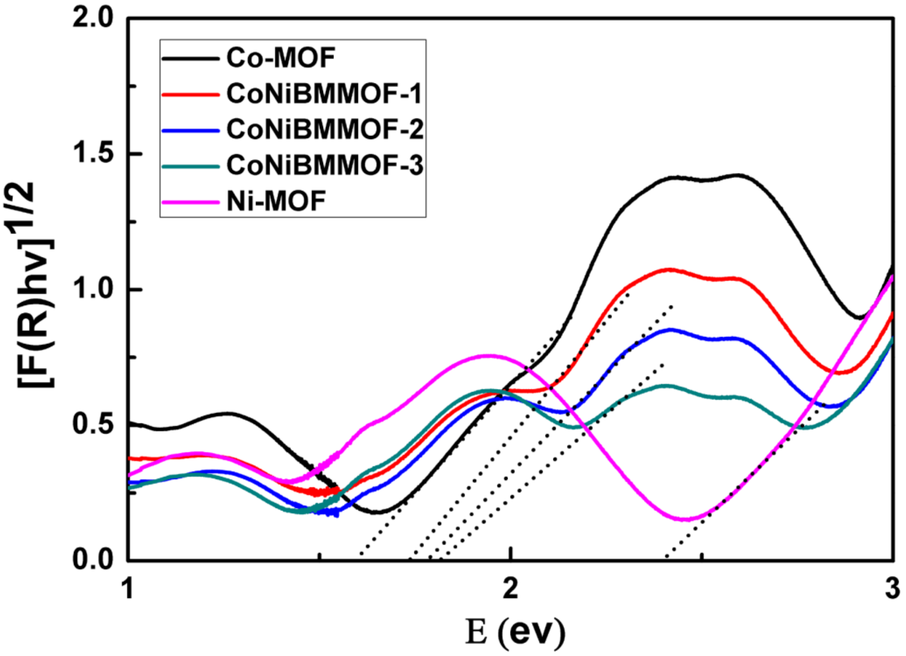


**Figure S3.** Plots of $(F(R)\,hv)^{1/2}$ *vs*. energy based on UV-Vis data for Co-MOF, CoNiBMMOF-1, CoNiBMMOF-2, CoNiBMMOF-3 and Ni-MOF, respectively.


**Figure S4.** Photographs showing the change of color of bimetallic MOF powders upon changing the molar ratio of the two metal nodes.

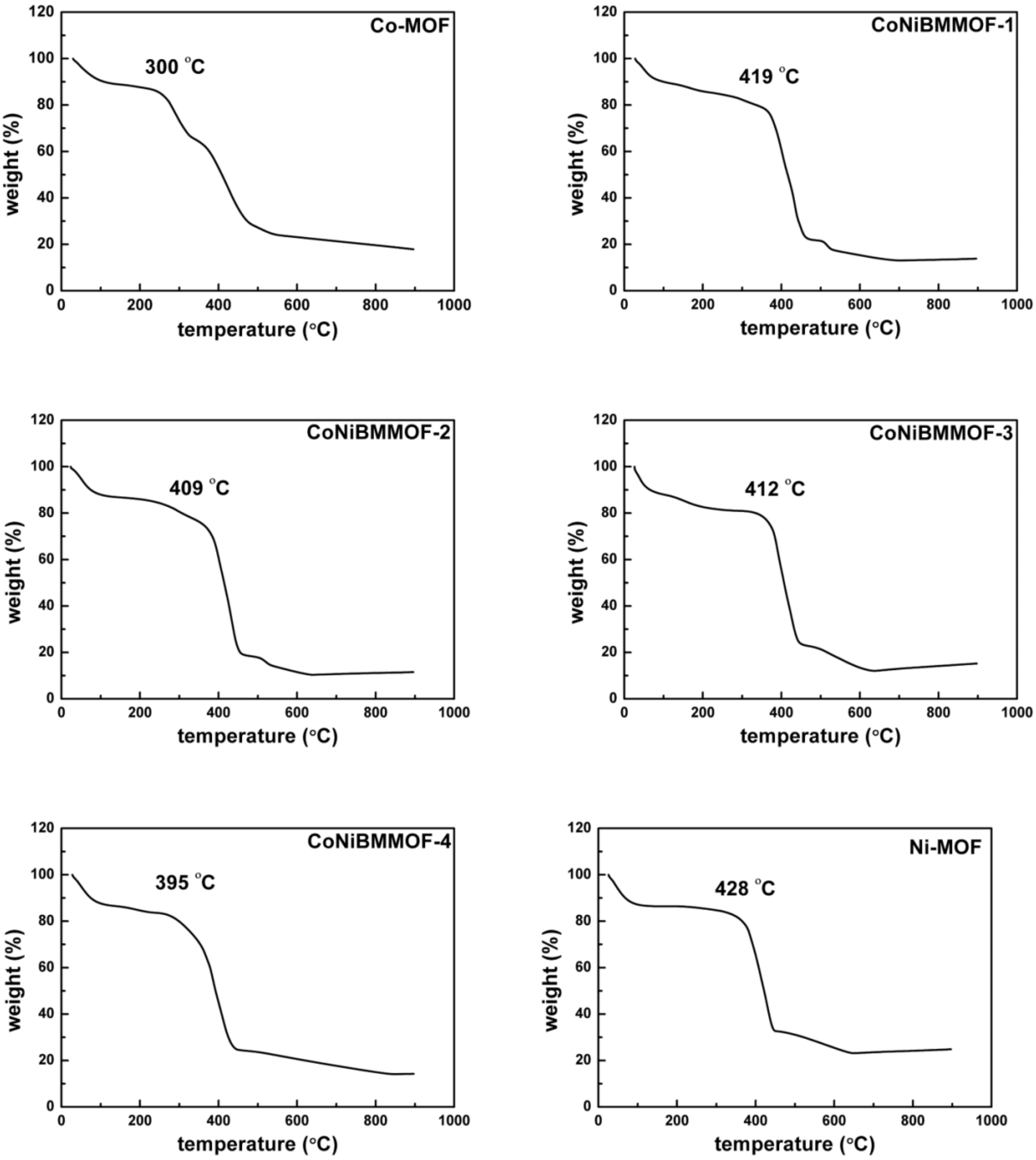


**Figure S5.** TGA traces and the decomposition temperatures of different M-bipy-BTC bimetallic MOFs under $N_2$ atmosphere. Heating rate: 5 ℃ $min^{-1}$.

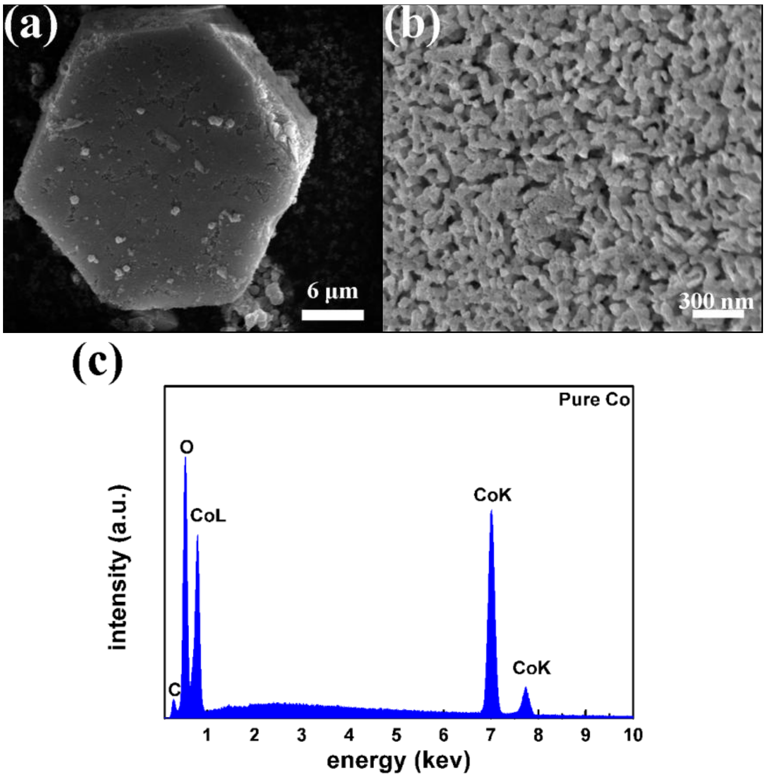


**Figure S6.** SEM images of Co@C at different magnifications with the scale bar of: (a) 6 μm and (b) 300 nm, respectively. (c) The corresponding EDS results.

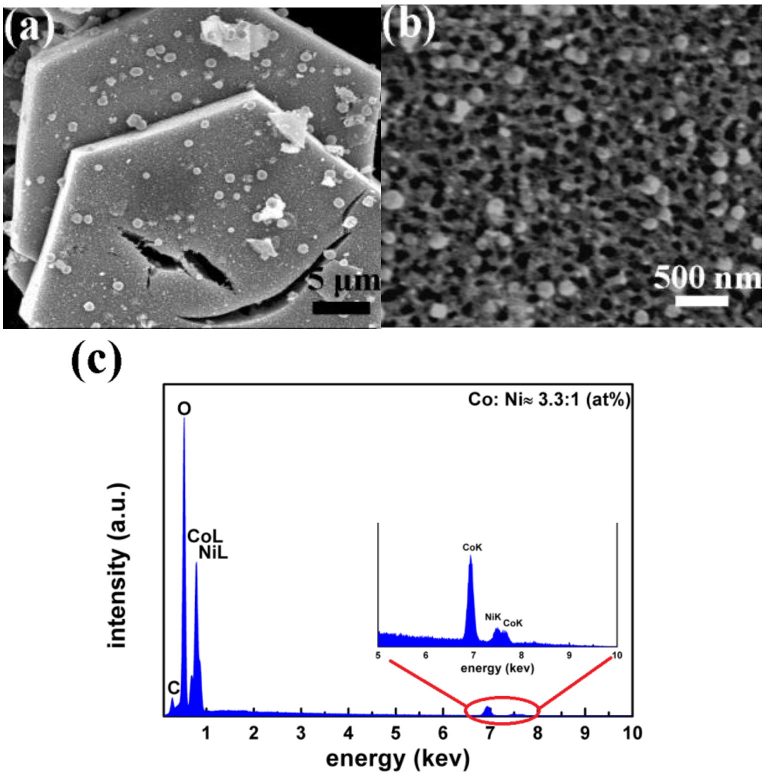


**Figure S7.** SEM images of CoNi1@C at different magnifications with the scale bar of: (a) 5 μm and (b) 500 nm, respectively. (c) The corresponding EDS results.

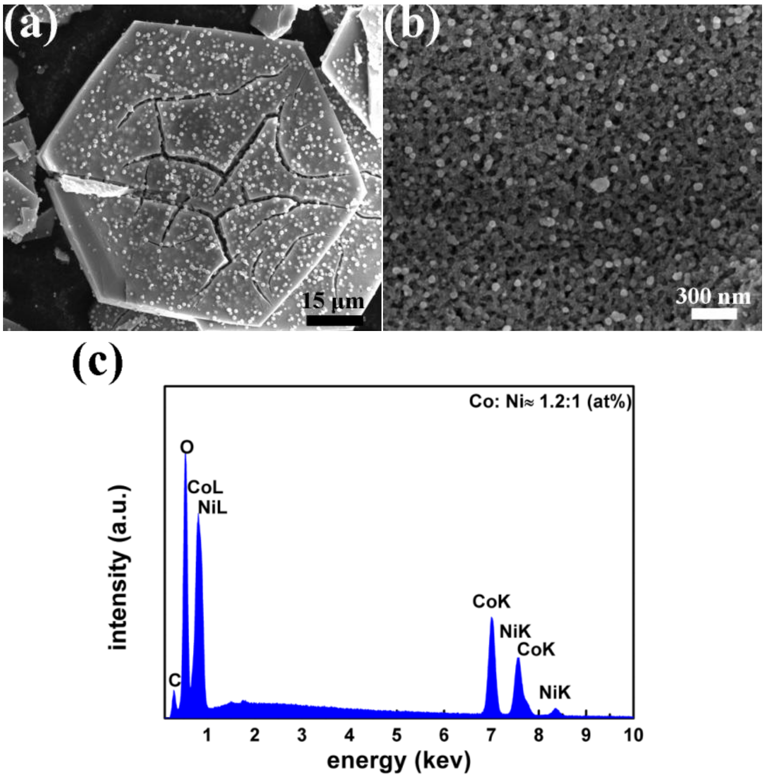


**Figure S8.** SEM images of CoNi2@C at different magnifications with the scale bar of: (a) 15 μm and (b) 300 nm, respectively. (c) The corresponding EDS results.

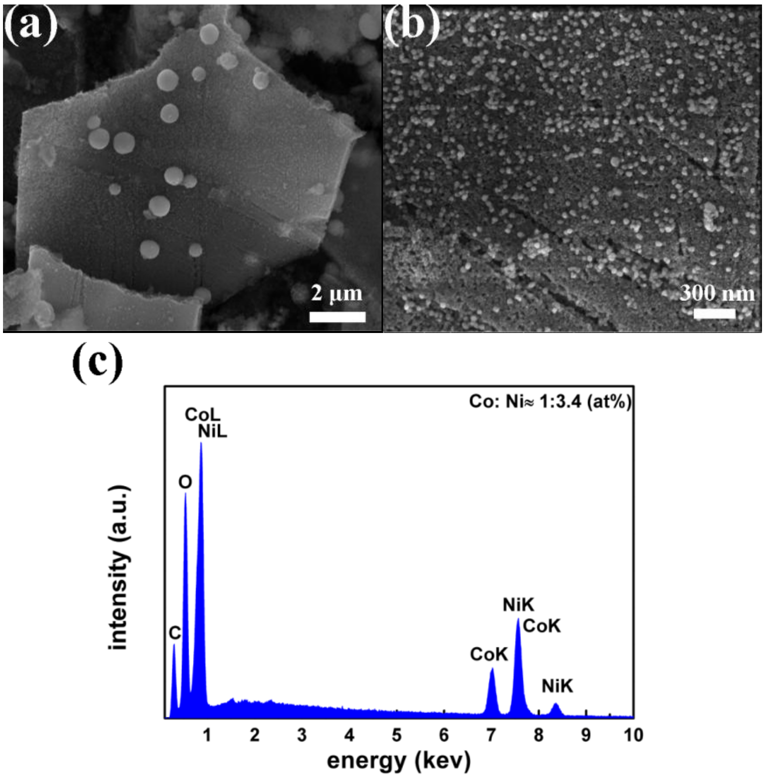


**Figure S9.** SEM images of CoNi3@C at different magnifications with the scale bar of: (a) 2 μm and (b) 300 nm, respectively. (c) The corresponding EDS results.

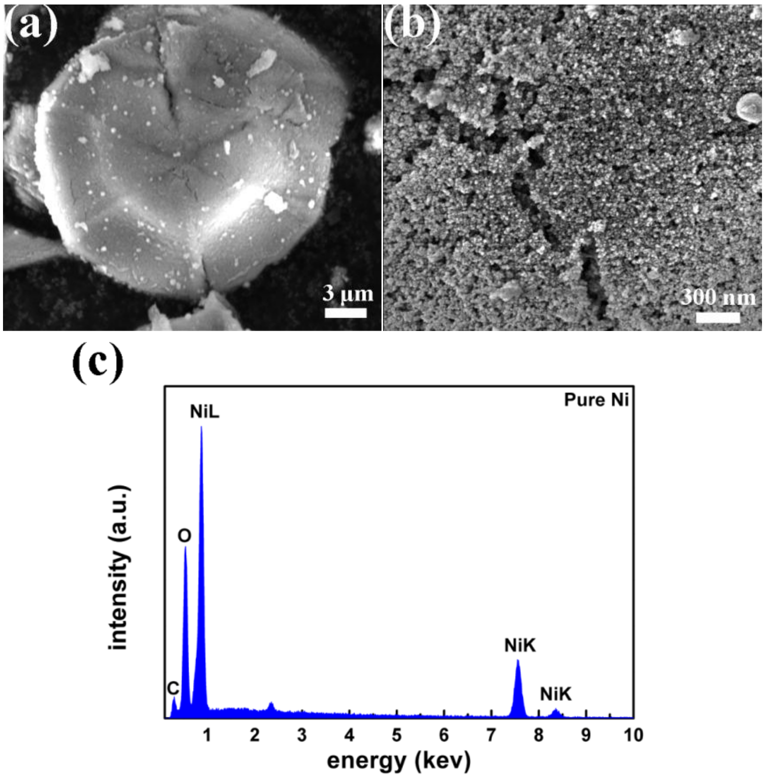


**Figure S10.** SEM images of Ni@C at different magnifications with the scale bars of: (a) 3 μm and (b) 300 nm, respectively. (c) The corresponding EDS results.

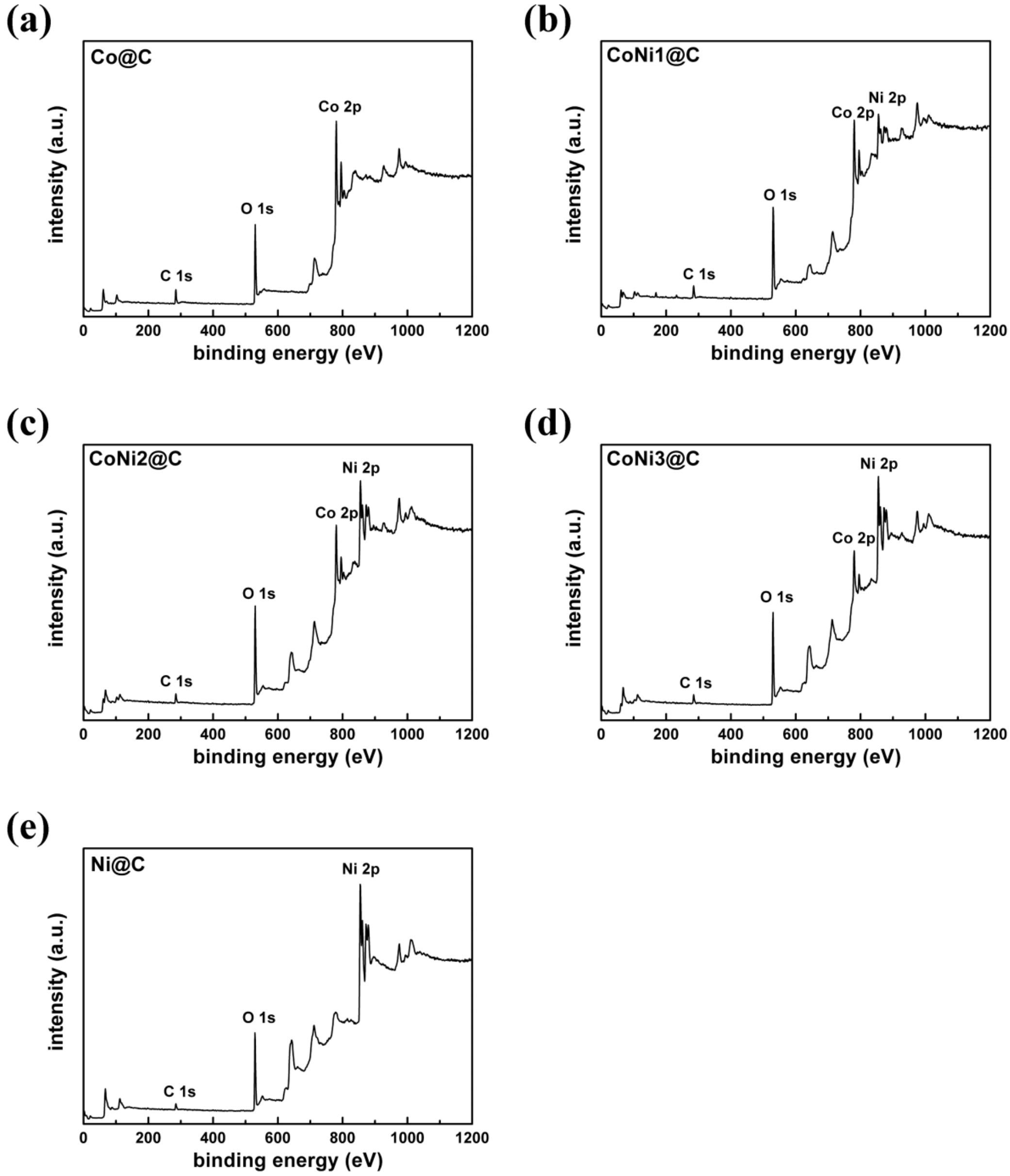


**Figure S11.** Full scan survey XPS spectra of different M-bipy-BTC bimetallic MOF derived catalysts

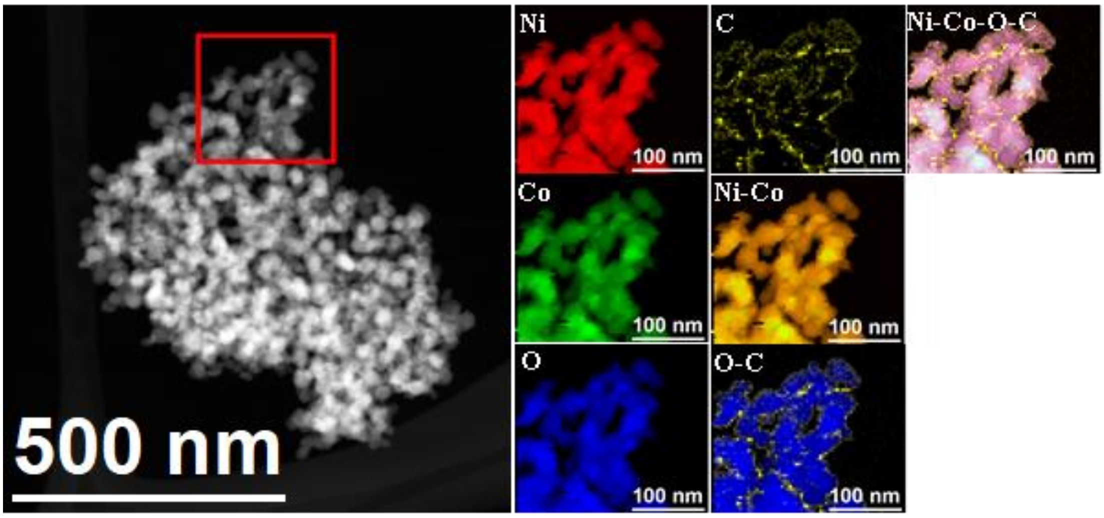


**Figure S12.** EELS chemical composition mapping of CoNi3@C obtained from the red squared area of the STEM micrograph, showing individual Ni $L_{2,3}$-edges at 855 eV (red), Co $L_{2,3}$-edges at 779 eV (green), O K-edge at 532 eV (blue) and C K-edge at 284 eV (yellow) as well as the composite (Ni-Co, O-C and Ni-Co-O-C) elemental mapping of this nanostructure.

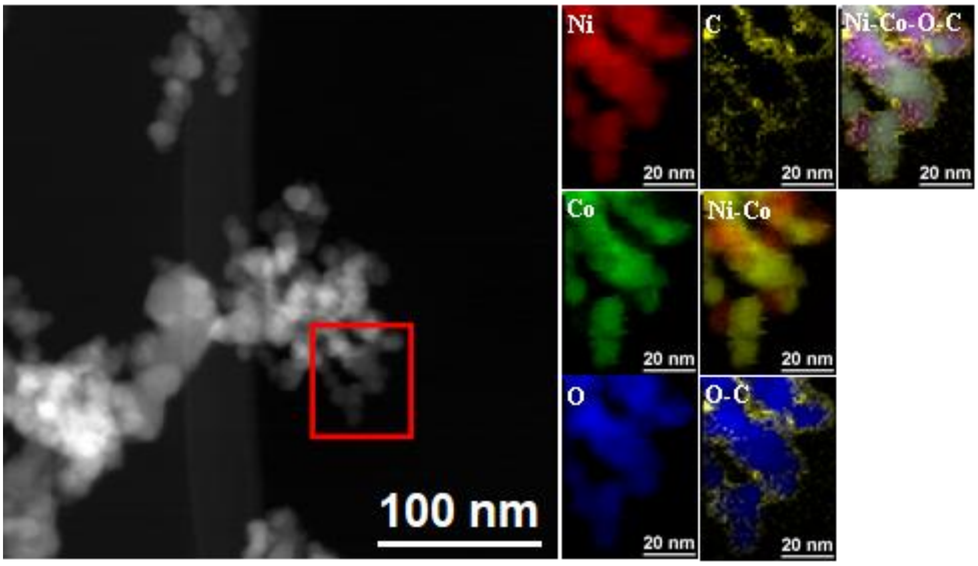


**Figure S13.** EELS chemical composition mapping of CoNi2@C obtained from the red squared area of the STEM micrograph, showing individual Ni $L_{2,3}$-edges at 855 eV (red), Co $L_{2,3}$-edges at 779 eV (green), O K-edge at 532 eV (blue) and C K-edge at 284 eV (yellow) as well as the composite (Ni-Co, O-C and Ni-Co-O-C) elemental mapping of this nanostructure.

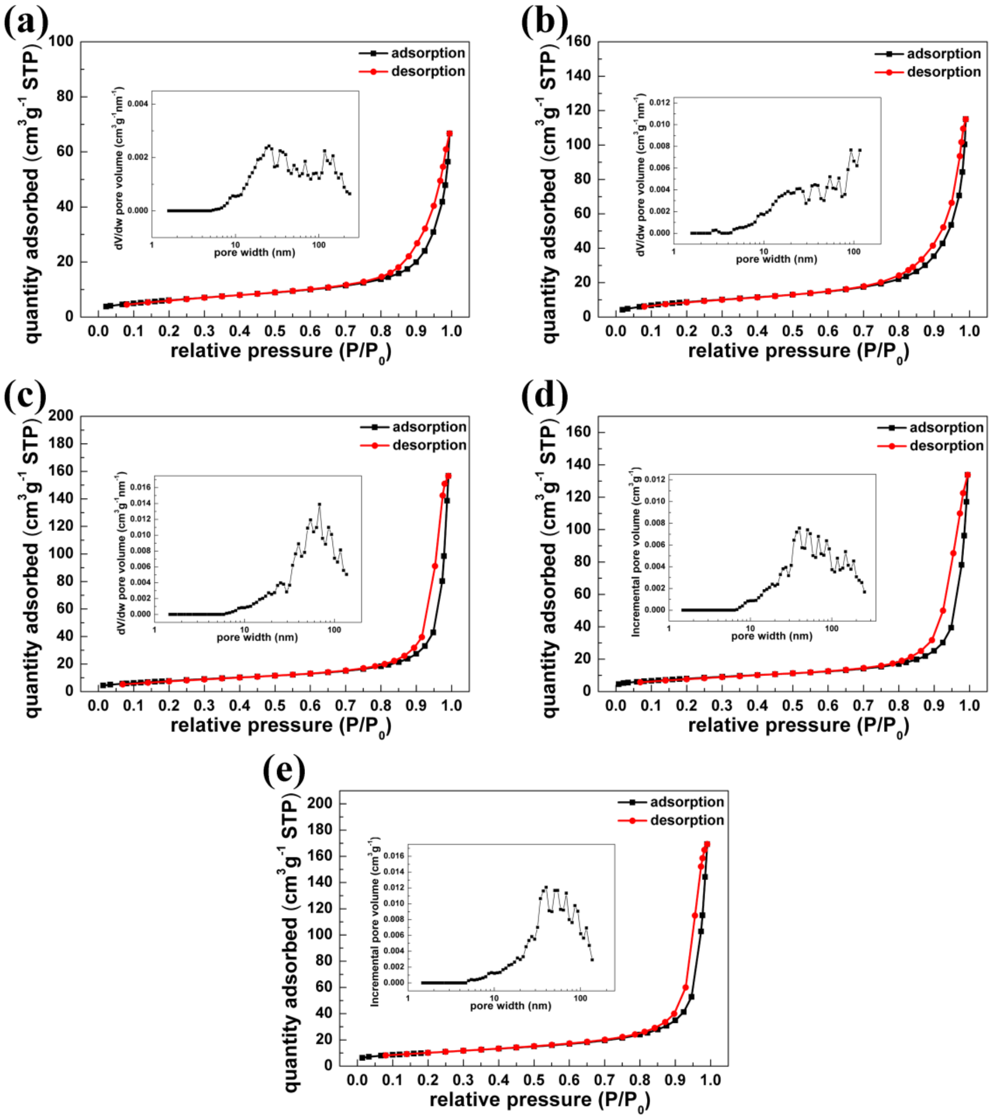


**Figure S14.** $N_2$ adsorption-desorption isotherms and pore size distributions (the inset) of (a) Co@C, (b) CoNi1@C, (c) CoNi2@C, (d) CoNi3@C and (e) Ni@C, respectively.

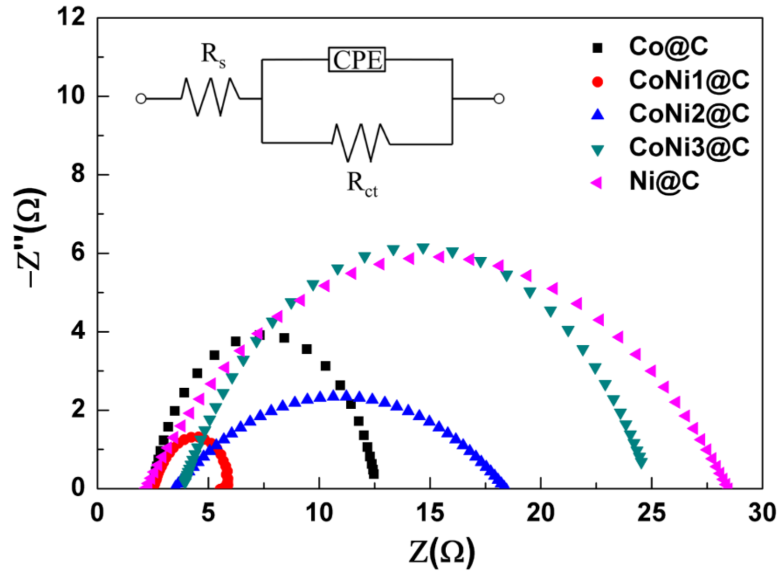


**Figure S15.** Nyquist plots of different catalysts (in the frequency range from 100 kHz to 0.1 Hz with an amplitude of 5 mV at $\eta$ = 380 mV). Inset: Modified Randles' equivalent circuit.

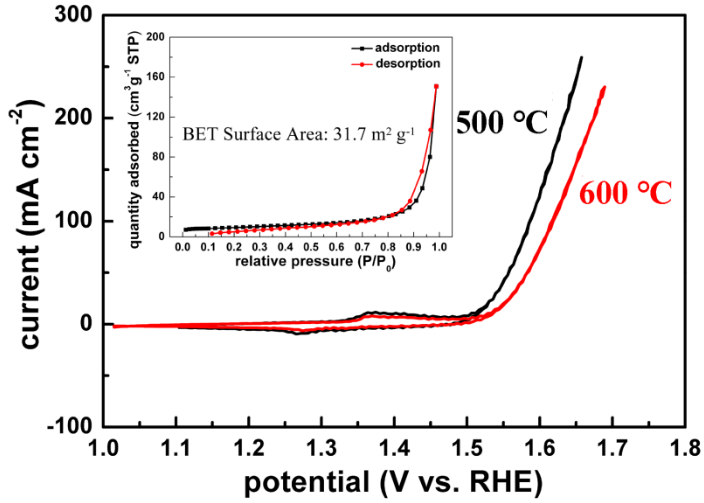


**Figure S16.** OER polarization curves of CoNi1@C (prepared under different pyrolysis temperatures) covered Ni foam in 1 M KOH in a three-electrode system; insert shows the $N_2$ adsorption-desorption isotherms of CoNi1@C, which was obtained under the pyrolysis temperature of 600 ℃.

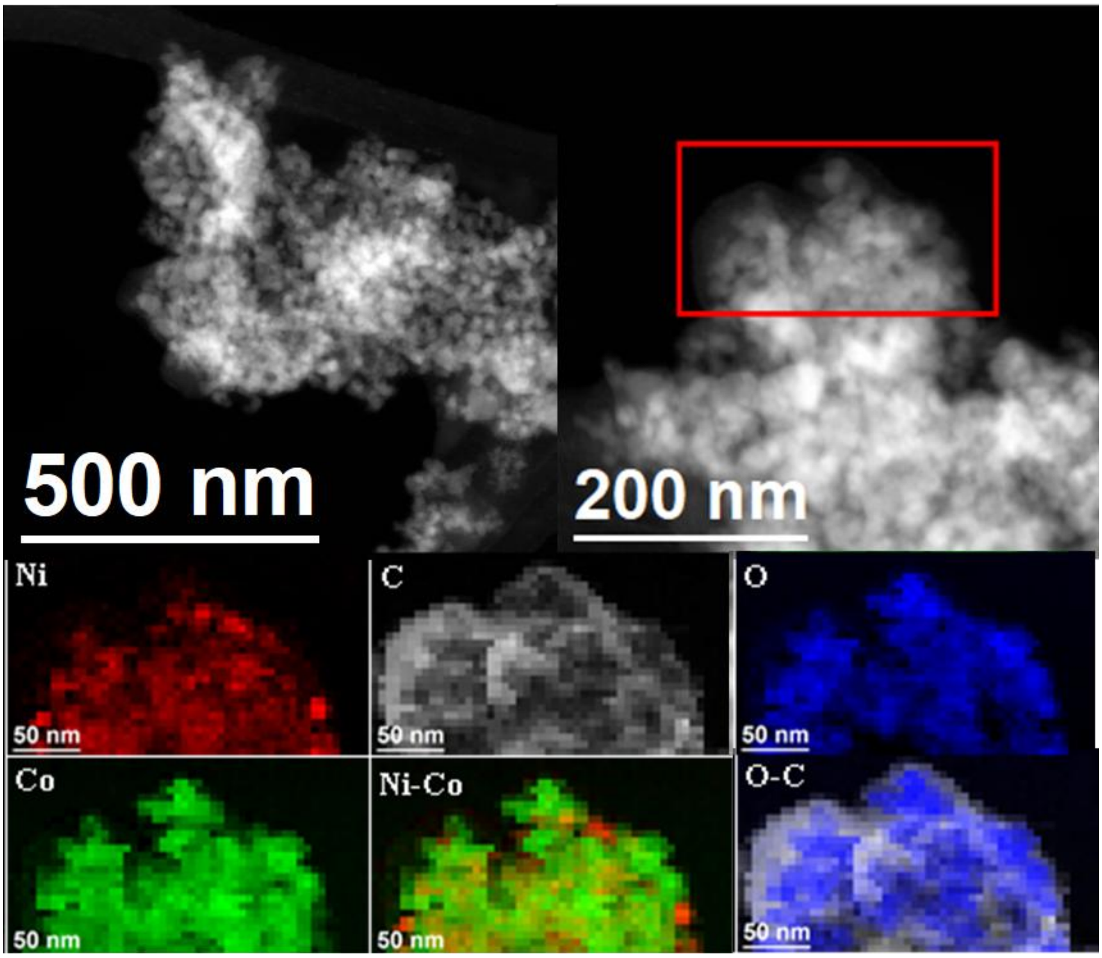


**Figure S17.** EELS chemical composition mapping of CoNi1@C after stability test obtained from the red squared area of the STEM micrograph. Individual Ni $L_{2,3}$-edges at 855 eV (red), Co $L_{2,3}$-edges at 779 eV (green), O K-edge at 532 eV (blue) and C K-edge at 284 eV (grey) as well as the composite (Ni-Co and O-C) elemental mapping of the this nanostructure.

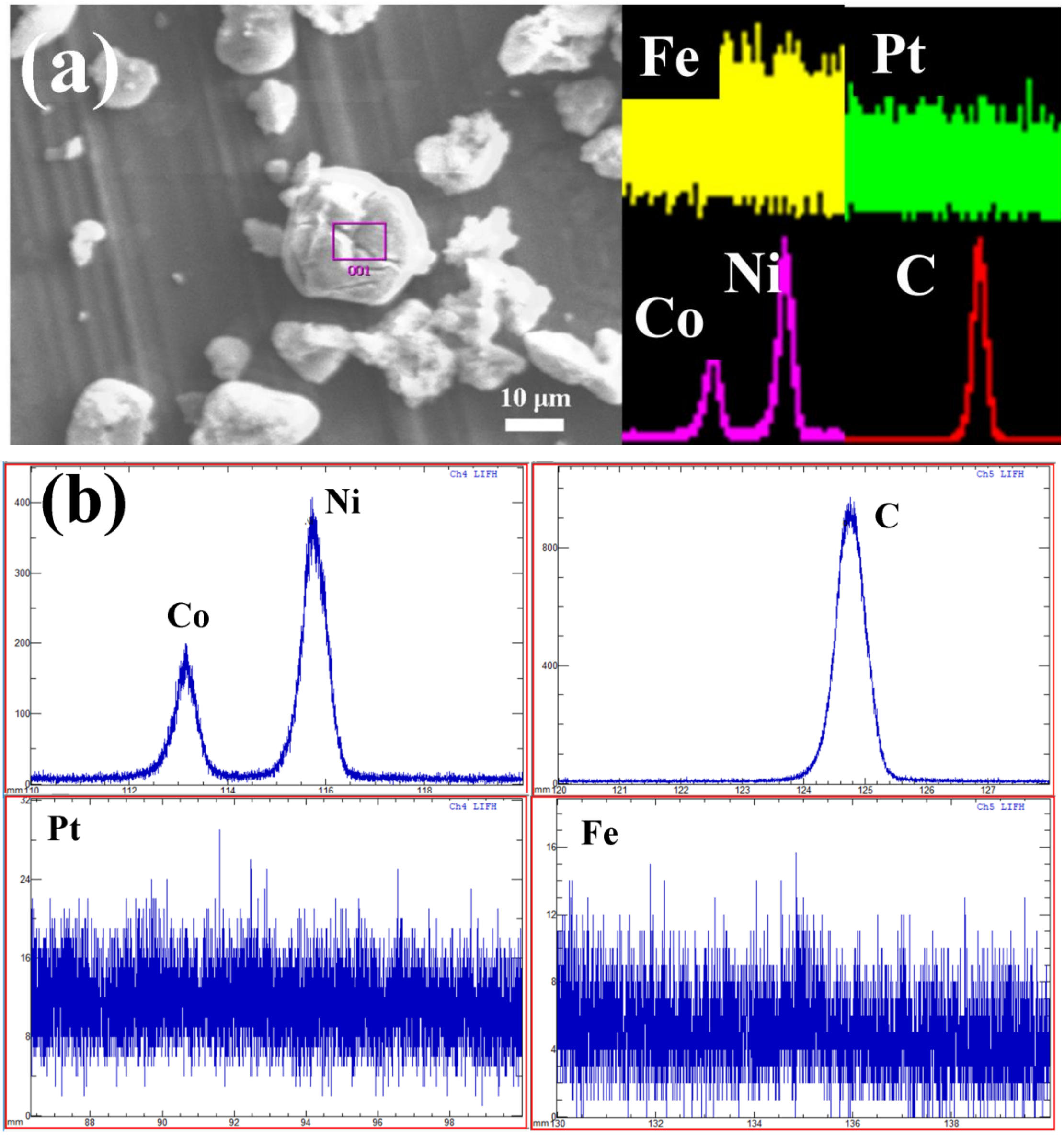


**Figure S18.** (a) SEM images and the corresponding WDS results for the catalyst CoNi1@C after 48 h durability test. (b) Scan details of WDS for different metal elements.

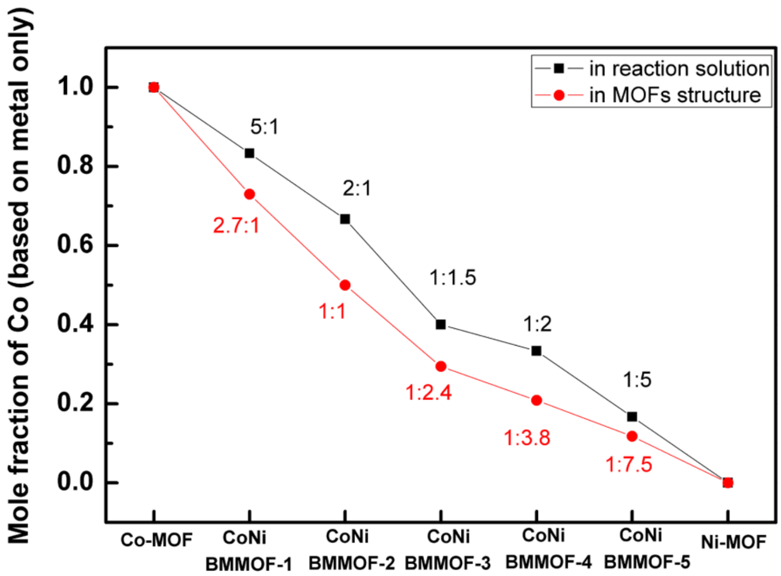


**Figure S19.** ICP-OES analysis results of the Co and Ni in the prepared MOFs (dissolved in 0.5 M HCL) and the corresponding reaction solution, wherein the mole ratio of Co *vs*. Ni in reaction solution and MOF structures is marked for each data point

**Table S1.** Elemental composition (atomic percentage) based on full scan survey XPS spectra analysis for different catalysts.

| | **C / at.%** | **O /at.%** | **Co / at.%** | **Ni / at.%** | **Co : Ni** |
|---|---|---|---|---|---|
| Co@C | 24.36 | 46.96 | 28.68 | 0 | Pure Co |
| CoNi1@C | 19.53 | 52.20 | 19.46 | 8.81 | 2.2:1 |
| CoNi2@C | 14.58 | 49.04 | 17.84 | 18.54 | 1:1 |
| CoNi3@C | 15.24 | 46.68 | 10.50 | 27.58 | 1:2.6 |
| Ni@C | 13.03 | 46.70 | 0 | 40.27 | Pure Ni |

**Table S2.** EIS fitted results of different catalysts (in the frequency range from100 kHz to 0.1 Hz with an amplitude of 5 mV at $\eta$ = 380 mV).

| | $R_s$ / Ω | Error / % | $R_{ct}$ / Ω | Error / % |
|---|---|---|---|---|
| Co@C | 2.5 | 1.0 | 10.1 | 2.2 |
| CoNi1@C | 2.6 | 0.4 | 3.4 | 0.8 |
| CoNi2@C | 3.5 | 5.3 | 16.8 | 2.9 |
| CoNi3@C | 3.7 | 1.6 | 21.1 | 2.0 |
| Ni@C | 1.6 | 5.2 | 27.5 | 1.8 |

**Table S3** Elemental composition based on WDS for the catalyst of CoNi1@C after 48 h durability test on different substrates (atomic percentage based on metal).

| | Co / at.% | Ni / at.% |
|---|---|---|
| CoNi1@C on Ni foam | 67.1 | 32.9 |
| CoNi1@C on carbon paper | 75.4 | 24.6 |

**Table S4.** Comparison of the electrochemical performance of Co-Ni mixed oxide catalysts in 1 M KOH for OER reported in the literature. The working electrodes are denoted as GC and NF for glassy carbon and Ni foam, respectively.

| Reference | Catalyst | Overpotential @$E_{OER@10\ mA\ cm^{-2}}$ | Overpotential @$E_{OER@100\ mA\ cm^{-2}}$ | Coating technique |
|---|---|---|---|---|
| **This work** | **CoNi1@C** | **335 mV (GC)** | **355 mV(NF)** | **Dip coating** |
| | | **276 mV (NF)** | | |
| Ref.21 | PBA derived Co-Ni (GC) | 380 mV | | Dip coating |
| Ref.22 | MOF-74 derived Co-Ni (GC) | ~560 mV | | Dip coating |
| Ref.S1[1] | $Co_9S_8$@NOSC | 340 (GC) | 420 (NF) | Dip coating |
| | | 330 (NF) | | |
| Ref.S2[2] | $Co_3O_4$/N-doped graphene | 310 (NF) | >370 (NF) | Dip coating |
| Ref.S3[3] | CoNi SUNOE | 450 (GC) | | Dip coating |
| Ref.S4[4] | Ni-Co-S/CF | | 363 (Copper foam) | Dip coating |
| Ref.S5[5] | $Co_3O_4$/N-doped graphene | 310 (NF) | >370 (NF) | Dip coating |
| Ref.S6[6] | NiCo-HS@G | 302 (NF) | 373 (NF) | Spray coating |
| Ref.S7[7] | Ni-P/Ni | | 374 (NF) | Direct growth |
| Ref.S8[8] | $Ni_3Se_2$ | | 388 (Copper foam) | Direct growth |
| Ref.S9[9] | $Ni_{2.3\%}$-$CoS_2$/C | | 370 (NF) | Direct growth |
| Ref.S10[10] | $NiCo_2S_4$ NA/CC | | 340 (NF) | Direct growth |
| Ref.S11[11] | Ni/$Ni_3N$ | | 470 (NF) | Direct growth |
| Ref.S12[12] | $Ni_3S_2$ | | 580 (NF) | Direct growth |
| Ref.S13[13] | NiO−Ni/NF | | 323 (NF) | Direct growth |
| Ref.S14[14] | $NiCo_2O_4$/$Ni_2P$ | 250 (NF) | ~350 (NF) | Direct growth |
| Ref.S15[15] | NiS/Ni | | ~370 (NF) | Direct growth |
| Ref.S16[16] | $Co_3O_4$@C-N NSA/NiF | | ~480 (NF) | Direct growth |
| Ref.S17[17] | $ZnCo_2O_4$ | | ~390 (NF) | Direct growth |
| Ref.S18[18] | $MnO_2$/$NiCo_2O_4$/NF | 340 (NF) | ~430 (NF) | Direct growth |
| Ref.S19[19] | 1D $NiCo_2S_4$ | 260 (NF) | ~375 (NF) | Direct growth |
| | $NiCo_2O_4$ | 330 (NF) | ~465 (NF) | |
| Ref.S20[20] | NF@Ni/C-600 | 265 (NF) | 467 (NF) | Direct growth |
| Ref.S21[21] | $Fe_2Cu_5Ni$ | 280 (NF) | 570 (NF) | Direct growth |
| Ref.S22[22] | P-$Ni(OH)_2$/$NiMoO_4$ | 270 (NF) | 380 (NF) | Direct growth |
| Ref.S23[23] | NiCoO@$Ag_{40}$/NF-Ar | | ~350 (NF) | Direct growth |
| Ref.S24[24] | $Co_3O_4$/$NiCo_2O_4$ (MOF) | 340 (NF) | ~495 (NF) | Direct growth |

**Table S5**. The preparation details of $Co_xNi_{1-x}$-BTC-DMF bimetallic MOFs.

| Samples | Molar ratio in reaction solution (Co : Ni) | Linker (gram per 100 mL) | Solvent |
|---|---|---|---|
| Co-BTC-DMF | Pure Co salt | 1.05 g | 80 mL DMF |
| $Co_xNi_{1-x}$-BTC-DMF-1 | 2:1 | 1.05 g | 80 mL DMF |
| $Co_xNi_{1-x}$-BTC-DMF-2 | 1:1 | 1.05 g | 80 mL DMF |
| $Co_xNi_{1-x}$-BTC-DMF-3 | 1:2 | 1.05 g | 80 mL DMF |
| Ni-BTC-DMF | Pure Ni salt | 1.05 g | 80 mL DMF |

The total concentration of metal salts is 5 mmol.

### *References listed in Supplementary Information:*


S1. S. Huang, Y. Meng, S. He, A. Goswami, Q. Wu, J. Li, S. Tong, T. Asefa and M. Wu, N-, O-, and S-Tridoped Carbon-Encapsulated $Co_9S_8$ Nanomaterials: Efficient Bifunctional Electrocatalysts for Overall Water Splitting. *Advanced Functional Materials* **2017,** *27* (17), 1606585.

S2. M. Tahir, L. Pan, R. Zhang, Y.-C. Wang, G. Shen, I. Aslam, M. A. Qadeer, N. Mahmood, W. Xu, L. Wang, X. Zhang and J.-J. Zou, High-Valence-State $NiO/Co_3O_4$ Nanoparticles on Nitrogen-Doped Carbon for Oxygen Evolution at Low Overpotential. *ACS Energy Letters* **2017,** *2* (9), 2177-2182.

S3. B. Ni and X. Wang, Edge overgrowth of spiral bimetallic hydroxides ultrathin-nanosheets for water oxidation. *Chemical science* **2015,** *6* (6), 3572-3576.

S4. T. Liu, X. Sun, A. M. Asiri and Y. He, One-step electrodeposition of Ni–Co–S nanosheets film as a bifunctional electrocatalyst for efficient water splitting. *International Journal of Hydrogen Energy* **2016,** *41* (18), 7264-7269.

S5. Y. Liang, Y. Li, H. Wang, J. Zhou, J. Wang, T. Regier and H. Dai, $Co_3O_4$ nanocrystals on graphene as a synergistic catalyst for oxygen reduction reaction. *Nature materials* **2011,** *10* (10), 780-786.

S6. T. Tang, W.-J. Jiang, S. Niu, N. Liu, H. Luo, Q. Zhang, W. Wen, Y.-Y. Chen, L.-B. Huang, F. Gao and J.-S. Hu, Kinetically Controlled Coprecipitation for General Fast Synthesis of Sandwiched Metal Hydroxide Nanosheets/Graphene Composites toward Efficient Water Splitting. *Advanced Functional Materials* **2018,** *28* (3), 1704594.

S7. C. Tang, A. M. Asiri, Y. Luo and X. Sun, Electrodeposited Ni-P Alloy Nanoparticle Films for Efficiently Catalyzing Hydrogen- and Oxygen-Evolution Reactions. *ChemNanoMat* **2015,** *1* (8), 558-561.

S8. J. Shi, J. Hu, Y. Luo, X. Sun and A. M. Asiri, $Ni_3Se_2$ film as a non-precious metal bifunctional electrocatalyst for efficient water splitting. *Catalysis Science & Technology* **2015,** *5* (11), 4954-4958.

S9. W. Fang, D. Liu, Q. Lu, X. Sun and A. M. Asiri, Nickel promoted cobalt disulfide nanowire array supported on carbon cloth: An efficient and stable bifunctional electrocatalyst for full water splitting. *Electrochemistry Communications* **2016,** *63*, 60-64.

S10. D. Liu, Q. Lu, Y. Luo, X. Sun and A. M. Asiri, NiCo2S4 nanowires array as an efficient bifunctional electrocatalyst for full water splitting with superior activity. *Nanoscale* **2015,** *7* (37), 15122-15126.

S11. M. Shalom, D. Ressnig, X. Yang, G. Clavel, T. P. Fellinger and M. Antonietti, Nickel nitride as an efficient electrocatalyst for water splitting. *Journal of Materials Chemistry A* **2015,** *3* (15), 8171-8177.

S12. S. Qu, J. Huang, J. Yu, G. Chen, W. Hu, M. Yin, R. Zhang, S. Chu and C. Li, $Ni_3S_2$ Nanosheet Flowers Decorated with CdS Quantum Dots as a Highly Active Electrocatalysis Electrode for Synergistic Water Splitting. *ACS applied materials & interfaces* **2017,** *9* (35), 29660-29668.

S13. Z. Yue, W. Zhu, Y. Li, Z. Wei, N. Hu, Y. Suo and J. Wang, Surface Engineering of a Nickel Oxide-Nickel Hybrid Nanoarray as a Versatile Catalyst for Both Superior Water and Urea Oxidation. *Inorganic chemistry* **2018,** *57* (8), 4693-4698.

S14. L. Wang, C. Gu, X. Ge, J. Zhang, H. Zhu and J. Tu, Anchoring $Ni_2P$ Sheets on $NiCo_2O_4$

Nanocone Arrays as Optimized Bifunctional Electrocatalyst for Water Splitting. *Advanced Materials Interfaces* **2017,** *4* (20), 1700481.

S15. W. Zhu, X. Yue, W. Zhang, S. Yu, Y. Zhang, J. Wang and J. Wang, Nickel sulfide microsphere film on Ni foam as an efficient bifunctional electrocatalyst for overall water splitting. *Chemical communications* **2016,** *52* (7), 1486-1489.

S16. X. Kuang, Y. Luo, R. Kuang, Z. Wang, X. Sun, Y. Zhang and Q. Wei, Metal organic framework nanofibers derived $Co_3O_4$-doped carbon-nitrogen nanosheet arrays for high efficiency electrocatalytic oxygen evolution. *Carbon* **2018,** *137*, 433-441.

S17. G. M. Tomboc, F. O. Agyemang and H. Kim, Improved electrocatalytic oxygen evolution reaction properties using PVP modified direct growth Co-based metal oxides electrocatalysts on nickel foam. *Electrochimica Acta* **2018,** *263*, 362-372.

S18. K.-L. Yan, X. Shang, W.-K. Gao, B. Dong, X. Li, J.-Q. Chi, Y.-R. Liu, Y.-M. Chai and C.-G. Liu, Ternary $MnO_2/NiCo_2O_4$/NF with hierarchical structure and synergistic interaction as efficient electrocatalysts for oxygen evolution reaction. *Journal of Alloys and Compounds* **2017,** *719*, 314-321.

S19. A. Sivanantham, P. Ganesan and S. Shanmugam, Hierarchical $NiCo_2S_4$Nanowire Arrays Supported on Ni Foam: An Efficient and Durable Bifunctional Electrocatalyst for Oxygen and Hydrogen Evolution Reactions. *Advanced Functional Materials* **2016,** *26* (26), 4661-4672.

S20. H. Sun, Y. Lian, C. Yang, L. Xiong, P. Qi, Q. Mu, X. Zhao, J. Guo, Z. Deng and Y. Peng, A hierarchical nickel–carbon structure templated by metal–organic frameworks for efficient overall water splitting. *Energy & Environmental Science* **2018,** *11* (9), 2363-2371.

S21. Y. Dong, F. Sun, X. Li, M. Chu, N. Li, X. Li, L. Wang, D. Qu, Y. Dong, Z. Xie, Y. Lin and C. Zhang, A Porous FeCuNi-Based Electrocatalyst Supported by Nickel Foam for Oxygen Evolution Reaction in Alkaline Conditions. *Journal of The Electrochemical Society* **2018,** *165* (14), F1127-F1132.

S22. W. Xi, G. Yan, H. Tan, L. Xiao, S. Cheng, S. U. Khan, Y. Wang and Y. Li, Superaerophobic P-doped $Ni(OH)_2/NiMoO_4$ hierarchical nanosheet arrays grown on Ni foam for electrocatalytic overall water splitting. *Dalton transactions* **2018,** *47* (26), 8787-8793.

S23. K.-L. Yan, J.-Q. Chi, Z.-Z. Liu, B. Dong, S.-S. Lu, X. Shang, W.-K. Gao, Y.-M. Chai and C.-G. Liu, Coupling Ag-doping and rich oxygen vacancies in mesoporous NiCoO nanorods supported on nickel foam for highly efficient oxygen evolution. *Inorganic Chemistry Frontiers* **2017,** *4* (11), 1783-1790.

S24. H. Hu, B. Guan, B. Xia and X. W. Lou, Designed Formation of Co(3)O(4)/NiCo(2)O(4) Double-Shelled Nanocages with Enhanced Pseudocapacitive and Electrocatalytic Properties. *Journal of the American Chemical Society* **2015,** *137* (16), 5590-5595.